Including Image Charge Effects in the Molecular Dynamics Simulations of Molecules on Metal Surfaces

F. IORI,[1] S. CORNI[2]
[1]*Department of Physics, University of Modena and Reggio Emilia, Modena, Italy*
[2]*INFM-CNR National Research Center on nanoStructures and bioSystems at Surfaces (S^3), Modena, Italy*

Received 10 October 2007; Revised 16 December 2007; Accepted 27 December 2007
DOI 10.1002/jcc.20928
Published online 19 March 2008 in Wiley InterScience (www.interscience.wiley.com).

Abstract: Combinatorial bio-techniques have demonstrated that proteins can be good and even selective binders for several inorganic surfaces, including metals. However, the understanding of the basic physical mechanisms that govern such interactions did not keep up with the success in these experiments. The comprehension of such mechanisms would greatly benefit from the computational investigation of the problem. Because of the complexity of the system, classical molecular dynamics simulations based on an atomistic description appear to be the best compromise between reliability and feasibility. For proteins interacting with metal surfaces, however, methodological improvements with respect to standard Molecular Dynamics (MD) of proteins are needed, since the polarization of the metal induced by the protein (and the surrounding water) is not generally negligible. In this article, we present a simple approach to introduce metal polarization effects (often termed image effects) in MD simulations by exploiting standard features of bio-oriented MD codes such as the widely used GROMACS and NAMD. Tests to show the reliability of the proposed methods are presented, and the results for a model application showing the importance of image effects are also discussed.

 J Comput Chem 29: 1656–1666, 2008

Key words: molecular dynamics; image charge; metal surfaces; adsorption; proteins

Introduction

The interaction of proteins with solid surfaces is a subject of great interest both for science and for technology. In fact, it has been experimentally demonstrated that proteins can be selected to have a remarkably (and in some cases even specific) affinity for several given inorganic surfaces.[1–3] The techniques used to select such proteins (cell surface[4] and phage display[5]) are based on a combinatorial approach: a huge protein library, containing up to 10^{12} different proteins, is driven to interact with the surface in several natural selection-like runs. Unfortunately, these approaches deliver some "winner" proteins but no information on the physical reasons behind such result. One of the surface that has been targeted by these combinatorial approaches is the Au(111) surface.[6,7] The interactions of proteins with such a surface are of interest for both biological applications (gold is the basis of the widely used Surface Plasmon Resonance technique to measure protein binding) and for potential nanobioelectronics applications.[8–10] Because of the complexity of the system (composed by a gold surface, a peptide or a protein and water), a full quantum mechanics approach is out of question and the only feasible atomistic method to study this system is classical Molecular Dynamics (MD). MD simulations of proteins/peptides on gold surfaces have been already performed in the literature,[11–14] as well as on other metals.[15] However, in all these articles one contribution to the total energy of the system has been neglected: the interaction of the solute and the solvent with the polarization that they induce in the metal (the *image charge* effect). This effect is usually deemed negligible (see the discussion in[16]) on the basis of estimates performed for pure liquids.[17–20] For example, the estimate in[20] was based on two assumptions that rely on the specific feature of the considered system (liquid ethanol): the solute was a neutral molecule (ethanol) and the solvent was considered to have a relatively high dielectric constant (24.3, bulk ethanol). Similarly, for pure liquid water on a metal surface, a large-scale cancellation of the image terms takes place,[16–19] an effect observed even in a water monolayer.[19]

Correspondence to: S. Corni; e-mail: stefano.corni@unimore.it

Contract/grant sponsor: EU, PROSURF; contract/grant number: FP6-NEST-028331

A strategy that aims to study a generic protein on a metal surface cannot rely on assumptions related to specific aspects of pure molecular liquids such as water or ethanol: The protein may have charged residues or even be globally charged, the medium directly surrounding the charged residues may have dielectric constant much lower than that of a bulk liquid, cancellation effects may not work in the presence of adsorbates. For example, the medium surrounding charges close to the surface can be the remainder of the protein (typical dielectric constant around 4) or the water layer in direct contact with the metal (a typically assumed dielectric constant for such a layer is 6[21]), or both. For a charged solute in a low dielectric medium image effect may be large: a simple electrostatic calculation for a monovalent ion at ≈4 Å from the metal surface in a medium with $\epsilon = 4$ gives an energy of ≈−20 kJ/mol. Image effects do not only create an attractive interaction between charges and the surface, they also affect mutual interactions between charges in the adsorbate. As an example (again based on simple electrostatics), for two monovalent ions 5 Å apart, both at 4 Å from the surface, the ion–ion electrostatic interaction energy is halved (for $\epsilon = 4$ it amounts to ≈ -40 kJ/mol). Thus, although for specific systems the neglect of these image effects may be justified *a priori*, this is not applicable as a general rule.

When the classical force field for metal–molecule interactions does not explicitly include a term to account for images, some of their effects might still be implicitly included in the remaining two-body metal-molecule parameters. This is the case of classical force fields lacking an explicit image term that have been parameterized to reproduce *ab initio* results for an adsorbate on a metal surface[22–24]. Since the *ab initio* results include the adsorbate-metal polarization interaction (the quality of description depending on the calculation details), the classical force field parameters are forced to take values that simulate, as good as they can, such interaction. However, image effects are not simply described by a two-body interaction between the metal and the molecule (we shall discuss this point deeper in the following). Thus, it is not clear how well effective two-body parameters, such as Lennard-Jones or Morse coefficients, can represent image effects in an ensemble of molecules nearby a metal surface.

One may think to different options to include image effects in the dynamic simulation of a biomolecule-metal system. Having discarded the full quantum mechanics approach (e.g., a Car Parrinello simulation of a biomolecule in water on a metal slab) due to the prohibitive computational cost, at least other two approaches described in the literature for metal/solution systems appear relevant. The first is to approximate the metal as an electron sea (described at the quantum mechanics level) interacting with a diffuse positive density of charge (jellium model). The description of image charge effects in the framework of the jellium model has been widely explored in the 70s–80s.[25–27] The jellium model has been used together with classical Density Functional (DF) theory to study the structure of metal/liquid interface for dipolar liquids[28] and electrolyte solutions.[29,30] Moreover, classical molecular dynamics simulations of water/jellium interfaces have been also performed.[19,31] We are not aware of simulations of this kind for biomolecules on metals.

The second approach, empirical in nature but less expensive from the computational point of view, is to explicitly include image effects as a part of the classical force field for the simulated system. The straightforward choice is to introduce a dedicated term, E_{im}, in the classical potential energy of the system. For a metal that occupies the semi-space $z < z_0$, and for atomic sites labeled with i and j having partial charges q_i and q_j and positions $\vec{r}_i$, $\vec{r}_j$ (see Fig. 1), classical electrostatics provides a simple expression for E_{im}:

$$E_{im} = -\frac{1}{2}\sum_{ij}\frac{q_i q_j}{\sqrt{(x_i - x_j)^2 + (y_i - y_j)^2 + (z_i + z_j - 2z_0)^2}} \quad (1)$$

In ref. 32, it is noted that such a term compares well to DFT interaction energies for a single charge close to the densily packed Al(111) surface, when the charge-surface distance is greater than 2.5 Å. The direct inclusion of E_{im} is possible (e.g.,[33] a simulation of the electrochemical double layer), but impractical for simulations of large systems because the computational load will then scale with the square of the number of atoms (however, note that in[33] explicit image charges and a 2D Ewald method are used, keeping the same scaling behavior as the unpolarizable system). In addition, the inclusion of E_{im} in widely used MD software oriented to biomolecules (e.g., AMBER, GROMACS, and NAMD) would require a modification of the original code (or, for NAMD, a cumbersome and system-specific Tcl/Tk scripting). Other techniques to introduce image effects in classical MD simulations have been proposed in the literature. An approach (called discrete classical model, DCM) has been developed by Finnis et al.,[32,34] and recently applied to the simulations of isopropanol on Pt(111) surface.[35] The essence of the method is to represent the polarization of the metal via induced charges and dipoles on each metal atom. Good results were obtained in comparison to LDA (local density approximation) calculations on various Al surfaces. Siepmann and Sprick made use of overlapping Gaussian charge distributions located on metal sites. The total charge associated with each Gaussian is a dynamical variable that is determined by imposing a fixed electrostatic potential. Such a constraint is imposed via an extended Lagrangian techniques.[36] These are computationally viable approaches; however, they require to modify the source code of the MD program. The aim of the present article is to present a method to take into account image charge effects in MD simulations of biomolecules on surfaces that (a) does not need any editing of the MD program source code; (b) keeps the same scaling behavior of the original code, and (c) has a similar accuracy as the methods already proposed.[32,34,36] Although (a) may seem an improper limitation, the complexity of nowadays codes (related to their efficiency and the richness of features), as well as the fast code development, prevents an efficient handling by groups different from the official developers. Instead, an approach that uses the normal input of the code is easier to perpetuate and to be exploited in different codes, and it is of certain impact in the user community.

Finally, we would like to stress that the model presented in this article is an empirical model, valid under the hypothesis already sketched in this Introduction and that will be detailed in the following. In particular, we had to sacrifice the realism of the quantum description of the metal response for a computationally faster, but more approximated, method, a trade-off which is also at the basis of classical MD simulations of biomolecules. Other empirical models could have been equally designed, as demonstrated by the discussion above.

Theory

Introducing the Method

The idea at the basis of our algorithm is that to reproduce the image effects it is not necessary to mimic the real physical mechanism, but only to reproduce its consequences. Thus, we shall not try to reproduce the complex nonlocal electronic effects that takes place in a metal subject to the electric field produced by the density of charge of a molecule nearby. Instead, we shall be satisfied with a computational strategy that reproduces just the metal polarization contribution to the potential energy surface of a molecule close to the metal. This approach fits well in the general philosophy of molecular mechanics, and, in particular, of polarizable force fields for classical MD,[37] where the electronic polarization of the molecule is approximated in classical ways. One of these classical approach is the so-called Drude oscillator (or shell) model,[38] where fictitious charged atoms (without van der Waals interactions) are added to the molecule topology, in such a way to create harmonic oscillators anchored to the molecule. The elongation of the oscillator gives origin to a dipole that simulates the electronic molecular polarization. In general, the typical time-scale of this polarization is much faster than nuclear motions. Thus, electronic polarization follows adiabatically the nuclear motion, a condition that is translated into molecular dynamics simulations by minimizing the energy of the Drude oscillators at each step (or every few steps) of the nuclear dynamics. Recently, it has been demonstrated (for polarizable water) that an extended system approach, where the Lagrangian of the system is extended to consider the oscillators as additional dynamical degrees of freedom, is also effective.[39] In principle, by wisely choosing the mass of the fictitious Drude oscillators and the time-step, it is possible to obtain an adiabatic decoupling of the nuclear motions and the oscillators, the latter keep vibrating (with a low T) around the proper minimum of their potential energy surface for each new nuclear configuration. This strategy is conceptually similar to the use of the fictitious electronic degrees of freedom in the Car Parrinello approach[40] to evolve the nuclear geometry and the ground state electronic wavefunction together.

Although such an approach (that also reproduces the right nuclear dynamics for the system) allows to save computational time with respect to the minimization, it would require unreasonably short time-steps to assure the proper adiabatic decoupling between the fictitious oscillators and the real nuclei dynamics. In addition, it may happen, for specific systems and/or for long simulations, that an efficient decoupling cannot be found, and the oscillators eventually thermalize with the rest of the system.

Improving the computational effectiveness of the oscillator approach requires to increase the computational time step up to the values commonly used for the unpolarizable system alone. However, this alone would have undesirable consequences for applications such as polarizable water. In fact, upon increasing the time step, one must also slow down (e.g., by increasing the mass) the dynamics of the fictitious oscillators, so to keep the numerical stability of the simulation. As a result, the fictitious oscillators and the real water are not adiabatically decoupled anymore, and energy would flow between them, spoiling the real dynamics of the system (essentially, a viscous drag would be added to the motion of water). Even when the real dynamics is not of interest, i.e., when one is interested only in averages or potentials of mean force, the use of long time steps and slow oscillators requires cautions: the oscillators heat up as the simulation proceed (since they are not decoupled from nuclear motions anymore), and unphysical forces (proportional to T) due to the correlation between oscillators arise,[39] preventing to simulate even the correct thermodynamics of the system. For all these reasons, in,[39] a low temperature thermostat is applied to the oscillators, so to keep them close to the minimum. With this expedient, the authors of[39] obtained, for liquid water, the same results as for the minimization approach, by using convenient unpolarizable-like time steps (0.5–2 fs).

These drawbacks in using oscillators with large time steps are only minor when we consider the specificity of the system under study. On one hand, most of the quantities that are interesting for proteins on surfaces (e.g., mean distances, orientations, potentials of mean force) are essentially averages, not requiring the knowledge of the real dynamics of the system. In addition, fictitious forces between polarizable gold atoms might be problematic only when the dynamics of the gold surface has to be simulated. Since surface deformations are likely smaller than those of the biomolecules, we shall keep the surface rigid (i.e., fictitious forces are simply neglected). Remarkably, when f ictitious forces are totally neglected, it is not necessary to impose a low T to the oscillator ensemble to minimize them. This is good because the use of low T for oscillators may artificially affect the energy distribution of the real system.

Our original idea to include gold polarizability was simply to apply the shell model, in the dynamical version with long time steps. However, we have found stability issues (discussed in Stability Issues for the Drude Oscillator Model) that prompted us to elaborate a second, more robust, model. We have thus implemented and tested two different polarizable gold atom models (Fig. 2).

Drude Oscillator Model

Following the original shell model, we added to the real gold atom a second interaction site connected by an harmonic bond with a force constant k and with a null rest length ($l_0 = 0$). Such an additional site has no van der Waals interactions with other atoms, is characterized by the mass m and the charge q. To keep the overall charge neutrality of the polarizable gold atom (original atom + virtual site), the original gold atom is assigned a charge $-q$. The electrostatic interaction between the two charges q and $-q$ on the same polarizable gold atom is not included in the energy and force calculations during the dynamics. This model requires to specify 3 parameters: k, q, and m. Their combinations define the quantities that determine the behavior of the polarizable gold atom: the polarizability $\alpha = q^2/k$ and the harmonic oscillator frequency $\omega = \sqrt{k/m}$ (Fig. 2 left).

Rod Model

A polarizable atom is also obtained by adding to the original gold atom a virtual interaction site that is forced to be at a given distance l_0 from the original atom, its orientation being free (Fig. 2 right). As for the Drude oscillator, the virtual site has no van der Waals interactions, while it bears a charge q ($-q$ is assigned to the original gold atom) and has a mass m. Unlike the Drude oscillator, this rod always has a finite dipole moment $\mu = ql_0$. Thus, it requires an orientational averaging (i.e., $T > 0$) to produce physically meaningful results. As for the Drude oscillator, the rod involves three parameters: l_0, q, and

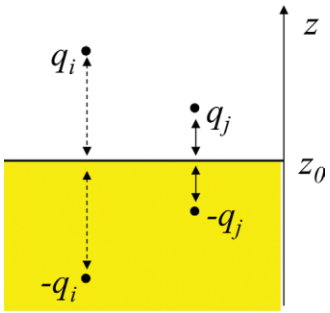

Figure 1. Scheme of the charge system described by eq. (1). The charges $-q_i$ and $-q_j$ inside the metal are the images of q_i and q_j, respectively.

m. In this case, however, the relation among the parameters and the characterizing physical quantities involve the temperature: the polarizability is given by $\alpha = \mu^2/3k_BT = q^2l_0^2/3k_BT$ while the typical intrinsic time-scale is determined by the rotation frequency at a given temperature, $\omega = \sqrt{2k_BT/(l_0^2 m)}$.

The statistical mechanics behind the Drude oscillator model has been discussed elsewhere.[39] For the rod model, the free energy F_E of the ensemble of N dipoles interacting with an external field $\vec{E}^{ext}$ is given by:

$$F_E - F_0 = -\frac{1}{\beta}\log\frac{\int d\hat{\mu}_1 \ldots d\hat{\mu}_N e^{\beta\sum_{i=1}^{N}\vec{\mu}_i\cdot\vec{E}_i^{ext}} e^{-\beta/2\sum_{i\neq j}\vec{\mu}_i\cdot T_{ij}\cdot\vec{\mu}_i}}{\int d\hat{\mu}_1 \ldots d\hat{\mu}_N e^{-\beta/2\sum_{i\neq j}\vec{\mu}_i\cdot T_{ij}\cdot\vec{\mu}_i}} \tag{2}$$

where $\vec{\mu}_i$ are the rod dipoles and T_{ij} is the standard dipole–dipole interaction tensor. Note that the integrals are done on the dipole orientations (i.e., on the unit vectors $\hat{\mu}_i$). By expanding to the second order in the external field, one finds:

$$F_E - F_0 = -\sum_i \langle\vec{\mu}_i\rangle_0\cdot\vec{E}_i^{ext} - \frac{\beta}{2}\sum_{ij}\vec{E}_i^{ext}\cdot(\langle\vec{\mu}_i\vec{\mu}_j\rangle_0 - \langle\vec{\mu}_i\rangle_0\langle\vec{\mu}_j\rangle_0)\cdot\vec{E}_j^{ext} \tag{3}$$

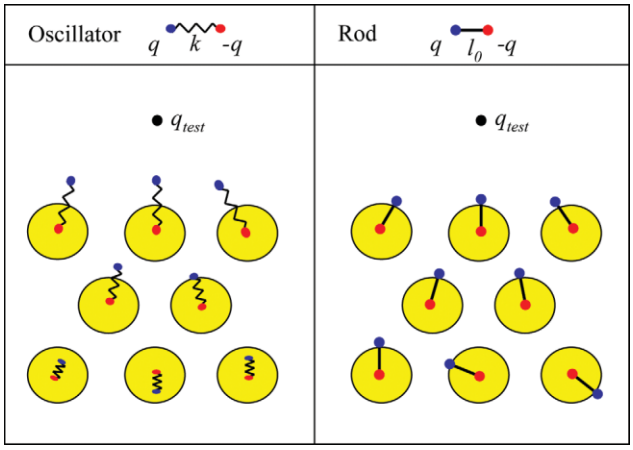

Figure 2. Scheme of the two gold polarizable models used in the present work.

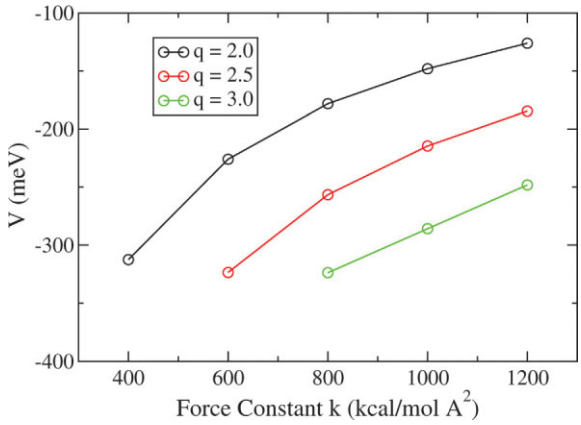

Figure 3. Potential at the point where the charge is located as a function of oscillator parameters.

where $\langle\ldots\rangle_0$ refers to the average over the dipole orientation performed at zero field. The first term, linear in E^{ext}, is null when each dipole averages to zero. This is a minimum requirement that it is not, however, automatically fulfilled. In fact, as we shall discuss in Choosing the Parameters for the Rod Model some choices for the dipole parameters may lead to an unphysical nonnull averaged dipole moment. The second-order term involves the dipole–dipole autocorrelation function, which is related to the static response function by the fluctuation–dissipation theorem.[41] Notably, if we neglect the dipole–dipole interaction term when performing the average, the autocorrelation function $\langle\vec{\mu}_i\vec{\mu}_j\rangle$ times β reduces to $\delta_{ij}\mu^2/3k_BT$, i.e., the expression reported above for the intrinsic dipole polarizability α.

If the average polarization of the dipole is linear with the applied field, a useful approximation can be obtained for the interaction free-energy F_{int} (see Appendix):

$$F_{\text{int}} = F_E - F_0 = \frac{1}{2}E_{\text{int}} \tag{4}$$

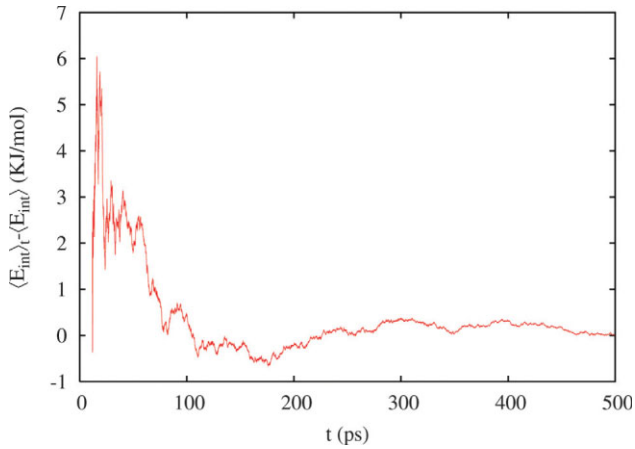

Figure 4. Running average of the interaction energy E_{int} for a single monovalent ion located 5 Å from a $5\sqrt{3} \times 7$ gold slab composed of 4-layers of rods.

where E_{int} is the interaction energy between the dipole system and the charge density that originate the field $\vec{E}^{ext}$.

Clearly, the use of polarizable dipoles to represent the metal polarizability does not allow to develop a net charge on the metal, as it happens for earthed conductors in the presence of external charges. In practice, we are limiting our approach to treat neutral, isolated metals. The extension to metals at an arbitrary potential would require the introduction of other quantities, such as net atomic charges on the metal atoms.

We would like to end this Section by commenting on a few issues that are present when simulating surfaces with common bio-oriented MD codes. Although a semi-infinite metal cannot be described with such codes, approximating the semi-infinite metal with a sufficiently thick slab does not introduce serious inaccuracies. A more subtle problem is how to treat a 2D periodic system, an issue explicitly addressed in the literature.[42] The option of using a fake periodicity in the third dimension (thus tracing back the overall problem to a 3D periodic system) should be used with caution, since it may cause deviations that persist even for cells with an asymptotically large size in the fake dimension.[43] Different solutions have been suggested, going from the addition of a simple corrective term to the total energy of the system[44] (that cures the wrong asymptotic behavior) to implementations of the Ewald sum in 2D.[45] All these solutions can be straightforwardly applied to polarizable gold surfaces within our approach.

In the present article, we did not correct for effects of the 3D periodicity because we compare our results with benchmarks, which also takes into account, at some level, the same fake 3D periodicity.

Results

Computational Details

All the calculations, unless otherwise stated, have been performed by considering a $5\sqrt{3}$x7 Au(111) surface (lattice parameter a_0 = 2.93 Å[46]) composed of four layers of gold. Slabs of this thickness are retained sufficient to quantum mechanically treat the adsorption of amino acids on gold.[46,47] The cell size in the direction perpendicular to the surface (z direction) was 50 Å. Calculations for the Drude oscillators model have been performed with NAMD 2.6[48] and GROMACS 3.3.1[49] (compiled in double precision). Calculations for the rod model have been performed only with GROMACS. In particular, the LINCS algorithm[50] has been used to constrain the rod length, and the motion of the original gold atoms (i.e., one of the rod ends) has been frozen.

All the simulations have been performed in the *NVT* ensemble. In particular, for NAMD calculations we used the Berendsen temperature coupling scheme,[51] while for GROMACS both the Nosè-Hoover[52,53] and the Berendsen algorithms have been tested, with similar results. PME (particle mesh Ewald)[54,55] has been used for electrostatic (based on a 1 Å step grid). Nonbonded interactions were cut off at 10 Å. To visualize and to analyze the results of the simulations, we used the VMD software[56] and the analysis programs included in GROMACS.

Stability Issues for the Drude Oscillator Model

We started our study by focusing on the Drude oscillator model, experimenting various force constants and charges and checking (a) the stability of the simulation and (b) the computed value of the electrostatic potential. In particular, we have considered a monovalent positive charge at distance 10 Å from the surface, and we have calculated the averaged electrostatic potential due to the Drude oscillators at the point where the charge sits. For these simulations, aimed at revealing stability issues, a large $18\sqrt{3} \times 27$ gold surface composed by six gold layers was used. Equilibration lasted 600 ps, followed by an accumulation period of 600 ps ($\Delta t = 1$ fs, m = 5 amu, $T = 300$ K). The results are reported in Figure 3. As it is evident from the figure, we were not able to find a combination of k and q that could give a value of the potential smaller than ~ -325 meV (the smaller is the potential, the closer the gold slab is to a conductor). From the k, q pairs that gave this lowest value, any attempt to decrease k or to increase q (i.e., increasing $\alpha = q^2/k$) resulted in an unstable simulation. Qualitatively, the instability of a Drude oscillator system can be understood by considering the overall potential at which the virtual gold atom is subject. Its expression contains a term in the form $kx^2/2 - q^2/|d - x|$ where $|d - x|$ is the distance from the virtual gold atom and the closest real gold atom belonging to a different oscillator. This energy has a barrier for a given x_b and then indefinitely decreases for $x \to d$ (we recall that no repulsive van der Waals is at work for the virtual atom). Clearly, if the virtual gold atom crosses the barrier, the simulation crashes. Since the probability of crossing such a barrier is always different from 0 (at $T > 0$), any simulation based on the finite temperature implementation of the Drude oscillators is doomed to crash at some point. However, when the barrier height is much larger than k_BT, the virtual charges has negligible probability of surmounting the barrier, and the simulation is stable for a sufficiently long time. Cooperative effects in the dipole ensemble may enhance this instability. Clearly, lowering the temperature stabilizes the dynamics,[39] since the surmounting of the barrier becomes less probable. Yet, we were not able to significantly improve on the results of Figure 3, even by choosing $T = 1$ K (and the proper Nosè-Hoover time parameter).

In addition, another form of (numerical) instability may be at work in our system: when the Ewald method (and methods based on it, such as PME) is used for calculating electrostatic forces, the interaction between the two charges that make the dipole cannot be directly neglected: it is necessary first to calculate the force due to all the charges in the system, and then to subtract the contribution from the other charge in the dipole. Since the charges can be very close, one ends up by using the difference of two large numbers as the instantaneous force, and thus numerical errors rapidly accumulate during the time evolution.

In the light of this discussion, the rod model, where the length of the rod is kept fixed by constraint algorithms such as LINCS, is an inherently more robust model with respect to oscillators. In fact, the fictitious moving charge cannot collapse on other charges, as it may happen for oscillators, and the rods can be chosen long enough to minimize the possible PME inaccuracy problem. In particular, we have performed via the rod model a simulation on a system identical to that used to obtain Figure 3, by using the rod parameters found in the next Section. The average potential due to rods at the point

Table 1. Total averaged dipole moment μ_{tot} for a 4 layers slab of rods that simulated the arrangement of a Au(111), $5\sqrt{3} \times 7$, surface, obtained in a 500 ps MD at $T = 300$ K.

q(au)	$\mu_{tot} \pm \sigma$(D)
0.2	0.16 ± 0.2
0.3	0.42 ± 0.92
0.4	3.27 ± 27
0.6	81 ± 0.6

The mass of the moving fictitious particle is 0.5 amu.

where the charge sits is −385 meV, a value ≈20% lower than what we could reach with oscillators.

On the basis of these considerations, we decided to give preference to the rod model, and in the following we shall focus on results from this model. In particular, rods have their peculiar sources of simulation instabilities, that will be discussed in the next section.

Choosing the Parameters for the Rod Model

The polarizability α of each single rod depends on the charge q, the length l_0 and the temperature T. The dynamics of the rod is also affected by the fictitious charge mass m, but the polarizability is not. For obvious reasons, it is convenient to keep the rod ensemble at the same T of the real system. We have thus explored the effect of other parameters for the most common temperature for protein-surface simulations, $T = 300$ K. The value of l_0 must be high enough not to give rise to inaccuracy in the electrostatics (our tests for the default PME settings in NAMD suggested >0.1–0.2 Å), but if l_0 is too long (>1 Å), it may clash with other fictitious charges or with atoms of the real system. Since α is affected by the product q and l_0, we can arbitrarily fix l_0 to a value in the reasonable interval 0.2−1 Å, and then play with the value of the charge q to optimize the polarizability. In particular, we have chosen $l_0 = 0.7$ Å, but tests with $l_0 = 0.3$ Å have been also performed (see Testing the Rod Model). Let us now discuss how q should be chosen. In principle, since we want to describe a conductor, one would expect that high α is needed, and thus high q. However, we should not forget that an ensemble of interacting orientable dipoles tends to align so to minimize their total energy, and this tendency becomes higher as the magnitude of each dipole increases. The resulting state is in general a disordered mix of domains, each with a defined dipole orientation. When the temperature is high enough, the boundary of each domains changes in time, as well as the orientation of the resulting dipole, giving on the average a null dipole moment for each rod, although cooperative effects can give non-negligible instantaneous total dipole moments. When the temperature is not high enough, the system behaves as a kind of glassy material, and the total dipole moment at zero field does not average to zero. We have indeed verified such behavior by monitoring the average total dipole moment as a function of the charge q, and the results are reported in Table 1. This "freezing" phenomenon gives an upper limit to the value of q, and, in turn, on the dielectric constant of the metallic slab. The highest q that does not show freezing is 0.3 (atomic units for the charge are used throughout this article). It gives a polarizability high enough to reproduce image charge effects, as described in the next Section.

Concerning the choice of q, we point out that the total dipole moment gives information about the system freezing, but the dipole moment of each single rod should also average to zero. To check if this is the case, for $q = 0.3$ we have randomly chosen 10 rods (five on the surface and five in the interior) and verified that, during the previous simulation, their value average to 0. The worse result was for a dipole located in the interior, that gave a negligible $|\langle\vec{\mu}\rangle|$ of 0.08 D ($\sigma = 0.04$). The temperature was also homogeneous (both with Nosè-Hoover and Berensen thermostat), as confirmed by analyzing the average kinetic energy of 10 randomly chosen rods.

Finally, we needed to choose the mass m of the fictitious charged site. The mass affects the typical dynamical times of the rod (the smaller the m, the faster the dynamics). Clearly, we would like to have the fastest dynamic that keeps the simulation stable (with the typical time step of $\Delta t = 2$ fs), so to minimize the total simulation time required to get reliable averages. However, a too fast dynamic would create instabilities in the constrain algorithm. In fact, typical algorithms employ iterative steps to correct unconstrained evolved coordinates in such a way that constraints are satisfied. If the unconstrained evolution gives rise to large changes in the coordinates of the rod ends (as it can happen for dynamics that are fast with respect to the time-step), the constraining algorithm will be unable to restore the rod length, the following evolution may lead to charge clashes and then simulation crashes.

We have performed some tests with different m (i.e., different time-scale for the rod dynamic) and the same time step $\Delta t = 2fs$ for a gold slab with a monovalent ion 1.3 Å (i.e., very close) to the surface. In these simulations (100 ps long) we monitored the bond length deviation after the unconstrained step (maximum and mean value among rods), and the typical time needed for the running average of the interaction energy to converge to ±1 kJ/mol of the final value. We tried masses from 0.1 amu to 2 amu. No one of the simulation crashed. We found that maximum deviations range from 5 Å (0.1 amu) to 0.2 Å (2 amu) and that mean deviations range from 1.4 Å (0.1 amu) to 0.07 Å (2 amu). Clearly, a 5 Å deviation is the signature of a too fast dynamic that could become unstable (however, even for such dynamics, we got the same mean interaction energy as for the slower dynamics, convergence to the final mean value in ≈10 ps and negligible rod length deviations after the LINCS step). On the other hand, $m = 2$ amu produced an interaction energy whose average did not converg to ±1 kJ/mol in 100 ps. We found that 0.5 amu is a good compromise, giving stable simulations (maximum observed deviation of 0.7 Å and mean deviation of 0.3 Å) together with convergence of the mean interaction energy for an ion close to the surface to ±1 kJ/mol of the final value in 50–100 ps. A typical running average of E_{int} for a rod simulation in the presence of a charge is reported in Figure 4.

As a matter of facts, at the date of resubmission of the present paper we have collected (in tests and on-going studies based on the rod model) several tens of nanoseconds of dynamics, without experiencing instability problems.

Testing the Rod Model: A Single Charge at Different Distances from the Surface

In classical MD simulations, the total density of charge of molecules (including the solvent ones) is approximated as a set of point charges placed at the positions of the nuclei, or at least in fixed positions with

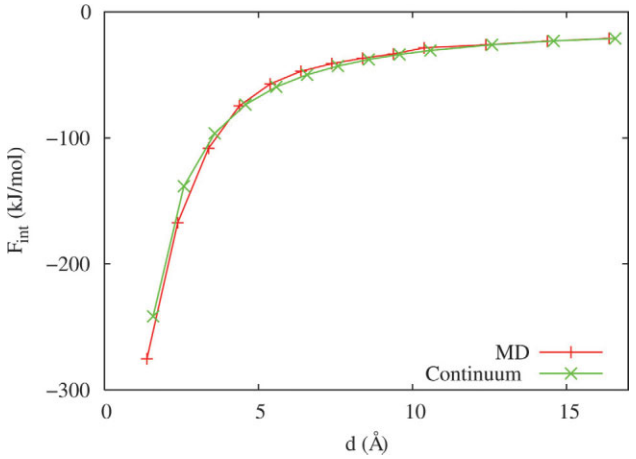

Figure 5. Interaction free energy of a test charge $q_{test} = -1$ with a Au(111) surface as a function of the gold-charge distance. "MD" refers to the MD rod results, and "Continuum" to results obtained for a charge in-between two conductors slab with thickness equal to the MD gold (111) slab. MD has been performed in the *NVT* ensemble with $T = 300$ K. For each point, 50 ps of equilibration + 450 ps of accumulation have been performed.

respect to them, having fractional values determined within a given parameterization procedure. It follows naturally that the first test for our model should be to check its ability to reproduce image (i.e., metal polarization) effects for just one point charge.

We have thus considered the interaction free energy [calculated via eq. (4)] of a single negative monovalent ion ($q_{test} = -1$) interacting with a four-layer slab of $5\sqrt{3} \times 7$ gold (111) as a function of

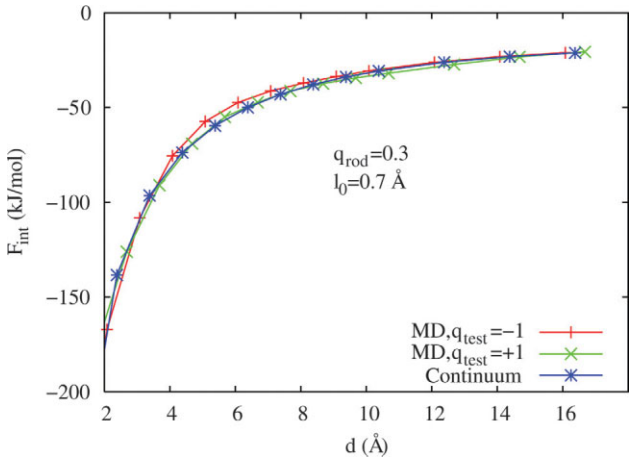

Figure 6. Interaction free energy of a positive and negative test charge with a Au(111) surface as a function of the gold-charge distance. "Continuum" refers to results obtained for a charge in-between two conductor slabs with thickness equal to the gold (111) slab. "MD" refers to the results obtained with the rod model with $q = 0.3$ and $l_0 = 0.7$ Å. The curve for $q_{test} = 1$ has been shifted by -0.3 Å while that for $q_{test} = -1$ has been shifted by 0.3 Å with respect to the continuum results. MD has been performed in the *NVT* ensemble with $T = 300$ K. For each point, 50 ps of equilibration + 50 ps of accumulation have been performed.

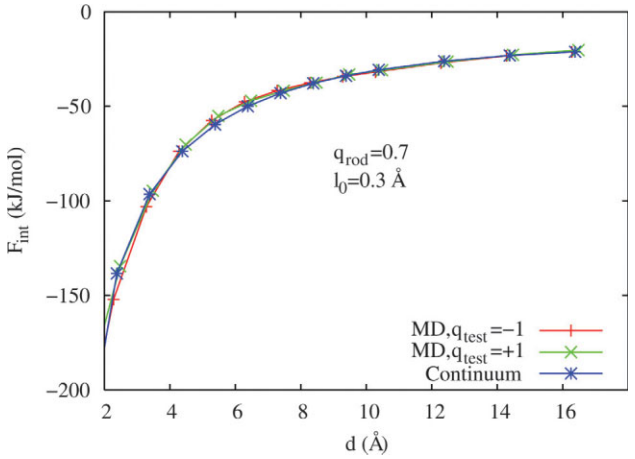

Figure 7. Interaction free energy of a positive and negative test charge with a Au(111) surface as a function of the gold-charge distance. "Continuum" refers to results obtained for a charge in-between two conductor slabs with thickness equal to the gold (111) slab. "MD" refers to the results obtained with the rod model with $q = 0.7$ and $l_0 = 0.3$ Å. The curve for $q_{test} = 1$ has been shifted by -0.1 Å while that for $q_{test} = -1$ has been shifted by 0.1 Å with respect to the continuum results. MD has been performed in the *NVT* ensemble with $T = 300$ K. For each point, 50 ps of equilibration + 50 ps of accumulation have been performed.

the surface-ion distance. These calculations have been performed by using the best q obtained in Choosing the Parameters for the Rod Model (i.e., $q = 0.3$ with $l_0 = 0.7$ Å). The benchmark to estimate our model should refer to the same system, a charge close to a finite metal slab with 3D periodic boundary conditions. Because of the fake periodicity along the surface normal z, q_{test} has non-negligible interactions with two slabs: one in the original cell and one in the closest replica along z. Thus, we chose to compare the rod results with the interaction energy obtained (by using a partial Fourier transform technique) for a point charge in-between two conductor slabs.

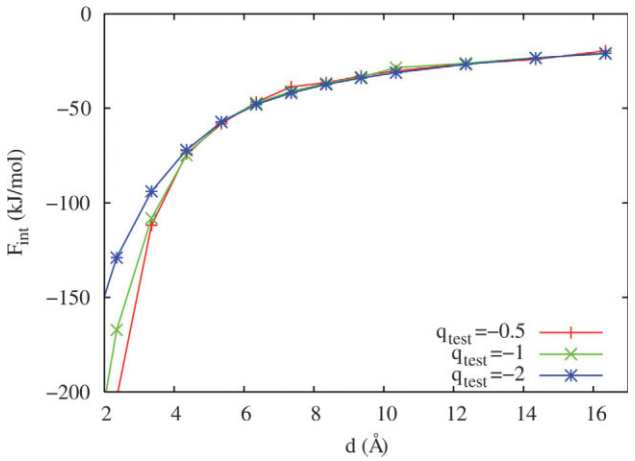

Figure 8. Interaction free energy for different values of q_{test}, as a function of the distance from a 4-layer Au(111) surface. All the curves have been renormalized to that of a unitary test charge. Each point has been obtained by performing 50 ps of equilibration + 50 ps of accumulation of MD in the *NVT* ensemble, $T = 300$ K.

Their positions mimic that of the gold layer in the original cell and in the replica closer to the charge. The periodicity in the surface plane is neglected in our benchmark. This should not be a bad approximation, since the charge is not moved in the x, y plane, but only along z. Finally, we have chosen the thickness of these two conductors to be equal to that of the gold slab (7.3 Å). The results from our model and the continuous dielectric benchmark are reported in Figure 5. Remarkably, the rod model reproduces well the continuum slabs results. The maximum difference between the model and the benchmark is ≈5 kJ/mol. Such a value is comparable with k_BT and surely negligible on the energy scale of the Figure.

Effects Related to the Finite Size of the Rods

To obtain the best matching between the continuum and the MD results in Figure 5, we had to introduce a small shift of +0.3 Å in the MD data, i.e., the image plane in MD is 0.3 Å outside the last layer of surface atoms. By fixing one end (the negative one in this case) of the rod, we have introduced a slight asymmetry in the dielectric response with respect to the test charge sign: when the test charge is negative, the mobile, positive ends of the rods protrude toward the charge, while for a positive test charge, the positive ends are repelled toward the metal interior. Thus, the mean position of the center of a rod is slightly displaced in opposite directions for positive or negative test charges, that results in a slightly different average distance between the charge and the rod centers.

The 0.3 Å shift is a consequence of such asymmetry. To check this point, we calculated the interaction energy for a positive monovalent ion, and we compared the results with the continuum ones (Fig. 6). To match the continuum results, we indeed have to shift the $q_{\text{test}} = 1$ curve by −0.3 Å, coherently with what found for $q_{\text{test}} = -1$. Clearly, the asymmetry in the response to charges of different sign can be removed by using rods whose center is fixed and both ends are mobile. The asymmetry can also be reduced by decreasing the rod length l_0. A test performed with $l_0 = 0.3$ Å and $q = 0.7$ (q has been changed to keep constant the product $q \cdot l_0 = \mu$) shows a negligible shift of ±0.1 Å and the same level of agreement between continuum and MD results as in Figure 6 (see Fig. 7).

Linearity of the Dielectric Response of the Rod Model

As a further check of the rod model, we have verified the magnitude of the deviation from linearity in the dielectric response of the slab. To this aim, we have repeated the calculation of Figure 5 for different values of q_{test}. In particular, we have considered $q_{\text{test}} = -0.5$ and $q_{\text{test}} = -2$. In Figure 8 the interaction free energy calculated via eq. (4) for each value of q_{test} is reported. All these energies have been linearly scaled to that of a monovalent ion (i.e., they should coincide in case of perfectly linear dielectric response of the rod ensemble). Notably, the curves for $q_{\text{test}} = -0.5$ and $q_{\text{test}} = -1$ agree quite well in the whole range of explored distances, showing that nonlinear effects are small for monovalent ions. However, the $q_{\text{test}} = -2$ results match the others only for $d > 4$ Å. Below this distance, the $q_{\text{test}} = -2$ curve gives interaction free energies that are smaller (in modulus) than what predicted for $q_{\text{test}} = -1$, suggesting that saturation of the dielectric response begins to take place. For $d \approx 2$ Å (smaller distances are unphysical in real systems), the deviation is ≈ 25%. When nonlinearity is present, F_{int} obtained by E_{int} via eq. (4) is not reliable. In particular, one expects that the correct F_{int} has a smaller absolute value than that estimated via E_{int}. By improving the estimate of F_{int} beyond eq. (4) (see Appendix), we found that the relative nonlinear deviation is actually ≈15%.

Although deviations from linearity are evident, they do not hinder the usefulness of the method: on one hand, this test has been conducted under "extreme" conditions (high net charges on a single atom, no solvent to screen the potential), while real applications to proteins present much milder conditions. On the other hand, nonlinearity to some degree is physically sound in the dielectric response of a metal to a nearby point charge.[32,34] In particular, the response of the metal should be decreased by this nonlinearity, as we also found in our classical model.

In conclusion, we have seen that the rod model is able to reproduce the interaction energy between a charge and a metal slab, although one must be aware of possible nonlinearities for high, unscreened charges. Equation 4, in these cases, may not give a good approximation to F_{int}. In the next Section we shall go one step further, by checking the ability of this model to reproduce one of the characterizing feature of the image charge interaction, i.e., that of modifying the mutual electrostatic interaction between ions nearby the metallic surface.

Two Charges on the Surface: Three-Body Effects in the Rod Model

One of the peculiarities of the image-charge interaction is that it effectively behaves as a three body interaction. This is made clear by eq. (1), where three sets of coordinates appear: those of two charges (i and j) and of the surface (z_0). In fact q_j is affected by the image charge of q_i, whose position is determined by the relative placement of q_i and the surface. Clearly, the ability of reproducing such a three body effect is an important requirement for our model. To verify that this is the case, we have considered a system composed by a gold (111) surface ($5\sqrt{3} \times 7$) mimicked by four layers of rods, a positive ion at a distance $d = 3.35$ Å from the closer dipole layer and a negative ion at the same distance from the surface. We have then varied the relative ion–ion distance (without changing the ion–surface distance) and calculated the mean total energy of the system (50 ps dynamics a $T = 300$ K). To extract the mean ion image interaction energy, we have subtracted from the mean total energy the direct ion–ion interaction energy. Then, we have assumed that the linear approximation holds (i.e., eq. (4) has been applied) and from the mean ion-image interaction energy we have obtained the interaction free energy. The results are shown in Figure 9, where we have also reported the ion image contribution calculated via a continuum model for the ion-gold distance d that best matches the MD results ($d = 2.5$ Å). In particular, this analytical interaction energy has been approximately calculated as the interaction of the two ions with their image charges in the original cell and in the closest replica in the xy plane. The z position of the ions is the same for all the points in the graph, so the effects of the periodicity in the z direction cancel out. The agreement between the MD and the continuum trends is very good, although we have to mention the discrepancy between the distance used in the MD calculations ($d = 3.35$ Å) and that in the best fitting analytical model ($d = 2.5$ Å). In a sense, the rod model seems to overestimate the indirect ion-ion interaction. However, we should not forget that the analytical benchmark accounts only approximately for the 3D periodicity of the MD system. In addition, it refers to a continuous dielectric, while the rod model is intrinsically discrete, so small discrepancies should not come as a surprise.

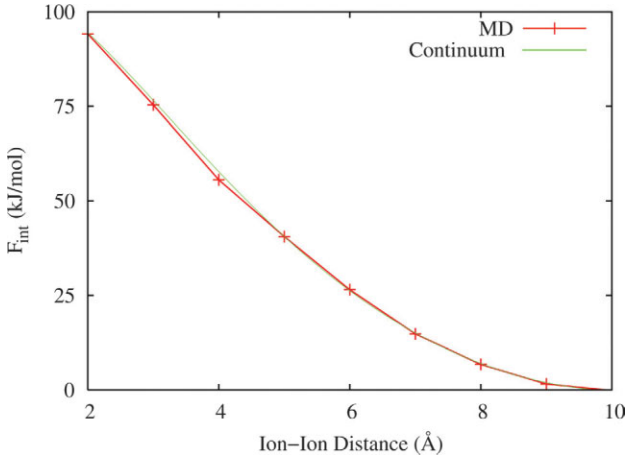

Figure 9. Image-charge contribution to the interaction free energy of two monovalent charges with opposite signs in front of a Au(111) surface. The gold-ion distance is 3.35 Å for both ions. Each point has been obtained by performing 50 ps of equilibration + 50 ps of accumulations at $T = 300$ K. A constant shift has been applied to F_{int} so to make the minimum value equal to 0. [Color figure can be viewed in the online issue, which is available at www.interscience.wiley.com.]

Application to a Model Molecule

The importance of the image charge effects on simulating proteins close to metallic surfaces should be assessed case by case for the protein under study. Here, we would like to demonstrate that including or not these interactions makes a difference for a prototypical system. To keep the model as simple and general as possible, we have considered a "molecule" with two sites. The two sites bear a charge of $+1$ and -1, respectively, and behave like large soft spheres (Lennard-Jones 6-12 potential). In particular, the largest site has $R_{vdW} = 5$ Å, while the other has $R_{vdW} = 1.7$ Å. The distance between the sites is constrained to 3 Å. All in all, this model system has electrostatic features similar to a polar amino acid on the surface of a small peptide, spherical on the average. This model system has been placed on a $5\sqrt{3} \times 7$ gold (111) surface composed by five layers and solvated with explicit water (the z size of the cell is 50 Å). We have fixed the largest site 4 Å away from the surface, leaving the other site free to evolve (with a mass of 20 amu). We have performed a 2-ns simulation (100 ps of equilibration plus 1.9 ns of accumulation) on this system, and we have finally analyzed the distribution of the angle θ between the direction that connects the two sites and the surface normal. The results, including or neglecting the image charge effects, are shown in Figure 10. We have chosen to plot the cosine of θ because a random orientation would appear on this cos scale as a line parallel to the base. A clear message emerges from this figure: image effects have important consequences on the orientation distribution, as proved by the differences between the two curves. In particular, the no-image distribution peaks at cos θ around 0.2 (i.e., $\theta \approx 80^o$), while the image distribution is almost constant (slightly increasing) between 0.2 and 0.8, having a sharp maximum close to 1 ($\theta = 0^o$). Both curves rapidly vanish for negative values of cos θ; this is simply due to the steric repulsion between gold and the mobile molecule site.

A complete rationalization of the differences between the two curves is not straightforward. In fact, not only the electrostatic preferences of the model molecules come into play, but also effects related to the interaction between the model molecule and water and between water and the surface (these latter are also affected by switching on and off the rod charges). Nevertheless, one point is clear: when image effects are neglected, the molecule has a tendency to lie as flat as possible on the surface, while when images are taken into account, the molecule prefers to stand up. A very simple continuum model can be used to understand these different behaviors: a dipole (representing the molecule) close to an interface between two dielectrics (see Fig. 11). The dipole is located in water, with $\epsilon \leq 80$ (as water close to an electrode) and the second medium has either $\epsilon \to \infty$ (image effects on) or $\epsilon = 1$ (image effects off). Standard electrostatics show that when $\epsilon \to \infty$ the dipole has a slight energetic preference for orienting perpendicularly to the interface, while for $\epsilon = 1$ the most favorable orientation is the parallel one, in qualitative agreement with our MD findings.

The reliability of the rod method for this model system is, in principle, guaranteed from the results of the tests presented in the previous sections, i.e., the ability of the method to reproduce image effects for charge-gold and charge-gold-charge interactions. However, we have also directly tested the method reliability for the studied system: The image E_{im} term in eq. (1) has been implemented in the MD program TINKER[57] (a serial program specifically designed with implementation easiness in mind), and the model system has been simulated for 2 ns. The results for the "molecule" orientation is depicted in Figure 12. In this figure, one can find the same basic difference between the "image on" and "image off" orientation distributions that we obtained in Figure 10 with the rod model: While for "image off" the probability peak is at cos θ around 0.2, for "image on" the peak location is close to 1, with a qualitatively similar behavior in other regions. Even the heights of these peaks compare well between the rod model and the benchmark. These findings back up the reliability of our model, and remark the importance of image effects in correctly describing adsorbate orientations on the surface. Some differences are visible, such as the magnitude

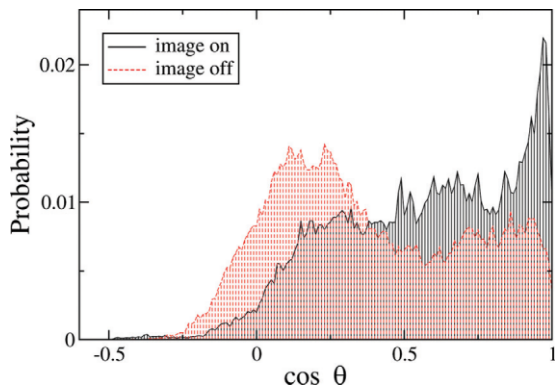

Figure 10. Distribution of the angle θ for a *NVT* MD simulation of the model system ($T = 300$ K) described in the text including ("image on") or neglecting ("image off") image charge effects via the rod method. [Color figure can be viewed in the online issue, which is available at www.interscience.wiley.com.]

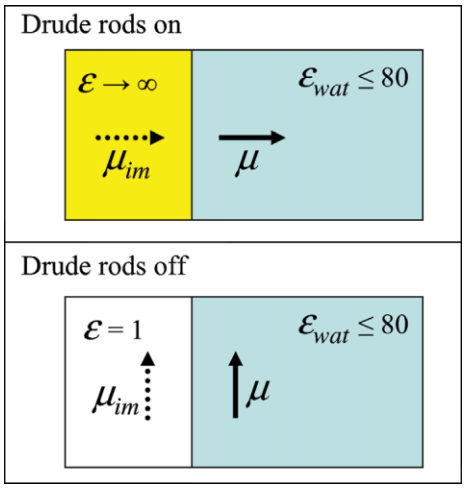

Figure 11. Scheme of the electrostatic model used to interpret Figure 10. When the rods are used ("Drude rods on"), gold behaves as a high-ε dielectrics, the interaction of the dipole μ with its image μ_{im} is favorable and the dipole prefers to stay perpendicular to the surface to maximize this interaction. When gold polarizability is neglected ("Drude rods off"), gold electrostatically behaves like vacuum, the interaction of μ with its image is unfavorable and the dipole prefers to stay parallel to the surface to minimize this interaction. [Color figure can be viewed in the online issue, which is available at www.interscience.wiley.com.]

of the "image off" distributions for $\cos\theta > 0.5$ and the somewhat more structured appearance of the "image on" results obtained in Figure 12 w.r.t Figure 10. These differences are likely related to statistical uncertainties in the distributions, which is reasonable if one considers that in producing each histogram in the graph only a subset of the simulation result is used. However, the overall agreement in the appearance of the distributions is remarkable, and provides a good indication of the reliability of the rod model.

Finally, we would like to stress that this example demonstrates that qualitatively wrong effects may be seen by neglecting the image-charge interaction in some cases. Features such as the correct orientation of amino acids on surfaces may not be captured. Since the image-charge interaction is physically part of the problem, it should be included, in general, in the description of the system.

Conclusions

In this article, we have presented a computational technique to empirically take into account image charge effects in classical molecular dynamics simulations of molecules on metallic surfaces. As mentioned in the introduction, other approaches have been proposed (and others could have been developed) to this aim. Our method has been particularly designed to be easily applicable in biological-oriented MD codes, without any need for source code modification. Different options for the model (Drude oscillator/rod) have been computationally investigated, and parameters apt to reproduce an high dielectric constant behavior have been worked out. Comparisons with continuum electrostatic estimates of the image effects have shown the usefulness of the model. At present we have found that the rod approach represents a robust and reliable model. It is worth mentioning that the model seems also to reproduce preliminary results obtained in our laboratory from periodic DFT calculations of organic ions on Au(111). In any case, the definitive validation of the model will certainly require an extensive comparison with well-controlled experimental results and accurate, first-principles, calculations.

Although the methods presented in this article have been confined to a version that is able to reproduce only free-energy profiles (i.e., not the real dynamics of the system), their inherent nature allows to be extended also to the simulation of the real time dynamics by carefully tuning the time-scale of the fictitious rod dynamics. The application of this method to a model system highlighted the importance of image effects in determining the molecular orientation on a surface. The study of real systems (e.g., proteins adsorbed on metallic surfaces) will clarify the actual importance of image-charge interactions in determining the strength and the specificity of the surface/molecule adduct, also in comparison with simulations for non-metallic substrates.[58–62]

Acknowledgment

The authors thank Giovanni Bussi for useful discussions and Rosa Di Felice for the careful reading of the manuscript. Discussions with PROSURF team members are also gratefully acknowledged.

Appendix: Free Energy Calculations Based on the Interaction Energy

Let us consider a system described by an Hamiltonian H_0 (the unperturbed rods in our case) where an interaction H_{int} (the interaction with the external field for our system) is switched on by a parameter λ, in such a way that $H(\lambda) = H_0 + \lambda H_{\text{int}}$. The mean interaction energy $E_{\text{int}}(\lambda)$ is given by:

$$E_{\text{int}}(\lambda) = \frac{\int dp\, dq\, \lambda H_{\text{int}} e^{-\beta(H_0+\lambda H_{\text{int}})}}{\int dp\, dq\, e^{-\beta(H_0+\lambda H_{\text{int}})}} \qquad \text{(A1)}$$

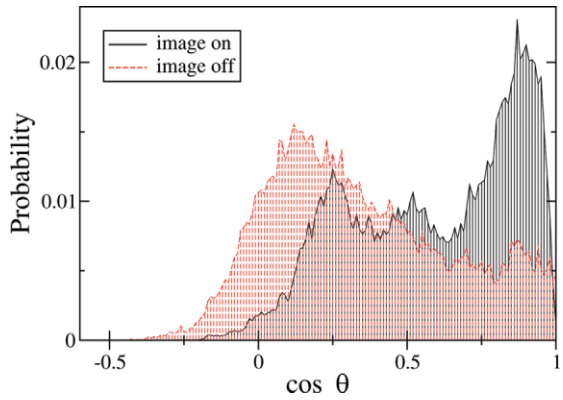

Figure 12. Distribution of the angle θ for a *NVT* MD simulation of the model system ($T = 300$ K) described in the text including ("image on") or neglecting ("image off") image charge effects via the E_{im} term of eq. 1. [Color figure can be viewed in the online issue, which is available at www.interscience.wiley.com.]

where q and p collectively indicate coordinates and momenta of the system. The free energy $F(\lambda)$ can be written (neglecting a constant):

$$F(\lambda) = -\frac{1}{\beta} \log \int dp\, dq\, e^{-\beta(H_0 + \lambda H_{\text{int}})} \tag{A2}$$

When H_{int} does not depend on λ (as for an external field acting on the rod ensemble, when the field magnitude is used as λ), eq. A1 can be re-written as:

$$E_{\text{int}}(\lambda) = -\frac{\lambda}{\beta} \frac{d}{d\lambda} \log \int dp\, dq\, e^{-\beta(H_0 + \lambda H_{\text{int}})} = \lambda \left. \frac{dF}{d\lambda} \right|_{\lambda} \tag{A3}$$

Exploiting this relation, one obtains:

$$F_{\text{int}}(\lambda) = F(\lambda) - F(0) = \int_0^{\lambda} d\lambda' \frac{E_{\text{int}}(\lambda')}{\lambda'} \tag{A4}$$

Equation A4 is valid both for linear and nonlinear response. In particular, when the response is linear, $E_{\text{int}}(\lambda)$ is quadratic in λ, i.e., $E_{\text{int}}(\lambda) = a\lambda^2$. By inserting such an expression in eq. A4, one promptly obtains eq. 4.

Equation A4 was also used to estimate the deviations from linearity of the rods ensemble response for a large test charge ($q_{\text{test}} = -2$) close to the surface ($d \approx 2$ Å), see Figure 8. In particular, E_{int} was calculated for different values of the charge q_{test} (that acts as λ), the resulting $E_{\text{int}}(q_{\text{test}})$ was fitted to a quartic polynomial in q_{test} and F_{int} for $q_{\text{test}} = -2$ was obtained by eq. A4.

References

1. Sarikaya, M.; Tamerler, C.; Jen, A. K.-Y.; Schulten, K.; Baneyx, F. Nat Mater 2003, 2, 577 and refs. therein.
2. Gray, J. J. Curr Opin Struct Bio 2004, 14, 110 and refs. therein.
3. Brown, S. In Nanobiotechnology; Niemeyer, C. M.; Mirkin, C. A. Eds.; Wiley: New York, 2004.
4. Wittrup, K. D. Curr Opin Biotechnol 2001, 12, 395.
5. Kehoe, J. W.; Kay, B. K. Chem Rev 2005, 105, 4056.
6. Brown, S. Nat Biotechnol 1997, 15, 269.
7. Brown, S.; Sarikaya, M.; Johnson, E. J Mol Biol 2000, 299, 725.
8. Alessandrini, A.; Salerno, M.; Frabboni, S.; Facci, P. Appl Phys Lett 2005, 86, 133902.
9. Alessandrini, A.; Corni, S.; Facci, P. Phys Chem Chem Phys 2006, 8, 4383.
10. Corni, S. IEEE Trans Nanotech 2007, 6, 561.
11. Braun, R.; Sarikaya, M.; Schulten, K. J Biomater Sci 2002, 13, 747.
12. Bizzarri, A. R.; Costantini, G.; Cannistraro, S. Biophys Chem 2003, 106, 111.
13. Bizzarri, A. R. Biophys Chem 2006, 122, 206.
14. Setty-Venkat, A.; Corni, S.; Di Felice, R. Small 2007, 8, 1431.
15. Oren, E. E.; Tamerler, C.; Sarikaya, M. Nano Lett 2005, 5, 415.
16. Shelley, J. C.; Bérard, D. R. In Reviews in Computational Chemistry, Vol. 12; Lipkowitz, K. B.; Boyd, D. B. Eds.; Wiley: New York, 1998.
17. Barabino, G.; Gavotti, C.; Marchesi, M. Chem Phys Lett 1984, 104, 478.
18. Spohr, E. Acta Chem Scand 1995, 49, 189.
19. Shelley, J. C.; Patey, G. N.; Bérard, D. R.; Torrie, G. M. J Chem Phys 1997, 107, 2122.
20. Qian, J.; Hentschke, R.; Knoll, W. Langmuir 1997, 13, 7092.
21. Hamann, C. H.; Hamnett, A.; Vielstich, W. Electrochemistry; Wiley-VCH: Weinheim, 1998.
22. Schravendijk, P.; van der Vegt, N. F. A.; Delle Site, L.; Kremer, K. ChemPhysChem 2005, 6, 1866.
23. Piana, S.; Bilic, A. J Phys Chem B 2006, 110, 23467.
24. Schravendijk, P.; Ghiringhelli, L. M.; Delle Site, L.; van der Vegt, N. F. A. J Phys Chem C 2007, 111, 2631.
25. Lang, N. D.; Kohn, W. Phys Rev B 1970, 1, 4555.
26. Lang, N. D.; Kohn, W. Phys Rev B 1973, 7, 3541.
27. Zangwill, A. Physics at Surfaces; Cambridge University Press: New York, 1988.
28. Bérard, D. R.; Kinoshita, M.; Ye, X.; Patey, G. J Chem Phys 1994, 101, 6271.
29. Bérard, D. R.; Kinoshita, M.; Ye, X.; Patey, G. J Chem Phys 1995, 102, 1024.
30. Bérard, D. R.; Kinoshita, M.; Ye, X.; Patey, G. J Chem Phys 1997, 107, 4719.
31. Schmickler, W.; Leiva, E. Mol Phys 1995, 86, 737.
32. Finnis, M. W. Surf Sci 1991, 241, 61.
33. Spohr, E. J Electroanal Chem 1998, 450, 327.
34. Finnis, M. W.; Kaschner, R.; Kruse, C.; Furthmüller, J.; Scheffler, M. J Phys Condens Mater 1995, 7, 2001.
35. Tarmyshov, K. B.; Müller-Plathe, F. J Chem Phys 2007, 126, 074702.
36. Siepmann, J. I.; Sprik, M. J Chem Phys 1995, 102, 511.
37. Ponder, J. W.; Case, D. A. Adv Prot Chem 2003, 66, 27.
38. Dick, B. G.; Overhauser, A. W. Phys Rev 1958, 112, 90.
39. Lamoureux, G.; Roux, B. J Chem Phys 2003, 119, 3025.
40. Car, R.; Parrinello, M. Phys Rev Lett 1985, 55, 2471.
41. Chandler, D. Introduction to Modern Statistical Mechanics; Oxford University Press: New York, 1987.
42. Frenkel, D.; Smit, B. Understanding Molecular Simulation; Academic Press: San Diego, 2002.
43. Spohr, E. J Chem Phys 1994, 107, 6342.
44. Yeh, I. C.; Berkowitz, M. L. J Chem Phys 1999, 111, 3155.
45. Widmann, A. H.; Adolf, D. B. Comput Phys Commun 1997, 107, 167.
46. Di Felice, R.; Selloni, A.; Molinari, E. J Phys Chem B 2003, 107, 1151.
47. Vargas, M. C.; Giannozzi, P.; Selloni, A.; Scoles, G. J Phys Chem B 2001, 105, 9509.
48. Phillips, J. C.; Braun, R.; Wang, W.; Gumbart, J.; Tajkhorshid, E.; Villa, E.; Chipot, C.; Skeel, R. D.; Kale, L.; Schulten, K. J Comp Chem 2005, 26, 1781.
49. van der Spoel, D.; Lindahl, E.; Hess, B.; Groenhof, G.; Mark, A. E.; Berendsen, H. J. C. J Comp Chem 2005, 26, 1701.
50. Hess, B.; Bekker, H.; Berendsen, H. J. C.; Fraaije, J. G. E. M. J Comp Chem 1997, 18, 1463.
51. Berendsen, H. J. C.; Postma, J. P. M.; DiNola, A.; Haak, J. R. J Chem Phys 1984, 81, 3684.
52. Nosè, S. Mol Phys 1984, 52, 255.
53. Hoover, W. G. Phys Rev A 1985, 31, 1695.
54. Darden, T.; York, D.; Pedersen, L. J Chem Phys 1993, 98, 10089.
55. Essmann, U.; Perere, L.; Berkowitz, M. L.; Darden, T.; Lee, H.; Pedersen, L. J Chem Phys 1995, 103, 8577.
56. Humphrey, W.; Dalke, A.; Schulten, K. J Mol Graph 1996, 14, 33.
57. Ponder, J. W. http://dasher.wustl.edu/tinker
58. Raffaini, G.; Ganazzoli, F. Langmuir 2003, 19, 3403.
59. Raffaini, G.; Ganazzoli, F. Macromol Biosci 2007, 7, 552.
60. Cormack, A. N.; Lewis, R. J.; Goldstein, A. H. J Phys Chem B 2004, 108, 20408.
61. Monti, S.; Carravetta, V.; Zhang, W. H.; Yang, J. L. J Phys Chem C 2007, 111, 7765.
62. Monti, S. J Phys Chem C 2007, 111, 6086.